Deformation Analysis to Detect and Quantify Active Lesions in 3D Medical Image Sequences

Jean-Philippe Thirion, Guillaume Calmon

INRIA

INSTITUT NATIONAL DE RECHERCHE EN INFORMATIQUE ET EN AUTOMATIQUE

Deformation Analysis to Detect and Quantify Active Lesions in 3D Medical Image Sequences

Jean-Philippe Thirion and Guillaume Calmon

N° 3101

Février 1997

THÈME 3

ISSN 0249-6399

INRIA
SOPHIA ANTIPOLIS

Deformation Analysis to Detect and Quantify Active Lesions in 3D Medical Image Sequences

Jean-Philippe Thirion and Guillaume Calmon

Thème 3 — Interaction homme-machine,
images, données, connaissances
Projet Epidaure *

Rapport de recherche n ° 3101 — Février 1997 — 38 pages

Abstract:

Evaluating precisely the temporal variations of tumor volumes is very important for at least three types of practical applications: pharmaceutical trials, decision making for drug treatment or surgery and patients follow-up. In this paper, we present a volumetric analysis technique, combining precise rigid registration of 3D medical images, non-rigid deformation computation and flow field analysis. Our analysis technique has two outcomes: the detection of evolving lesions and the quantitative measurement of volume variations. The originality of our approach is that no *precise* segmentation of the lesion is needed but the approximative designation of a region of interest, which can be automatized. We distinguish between tissue transformation (image intensity changes without deformation) and expansion or contraction effects reflecting a change of mass within the tissue; a real lesion being generally the combination of both effects. The method is tested with synthesized 3D image sequences and applied, in a first attempt to quantify in-vivo a mass effect, to the analysis of a real patient case with Multiple Sclerosis.

Key-words: motion field analysis, 3D image processing, 3D deformable grid, Multiple Sclerosis, volume measurement, tumor, mass effect, stereology

* http://www.inria.fr/Equipes/EPIDAURE-eng.html

Unité de recherche INRIA Sophia Antipolis
2004 route des Lucioles, BP 93, 06902 SOPHIA ANTIPOLIS Cedex (France)
Téléphone : 04 93 65 77 77 – Télécopie : 04 93 65 77 65

(Résumé : tsvp)

Analyse de déformations pour détecter et quantifier les lésions évolutives dans les séquences d'images 3D

Résumé : L'évaluation précise des variations temporelles du volume des tumeurs est importante pour au moins trois types d'applications pratiques : les essais pharmaceutiques, la prise de décision pour le traitement par des médicaments ou pour une chirurgie, et le suivi de patients. Dans cet article, nous présentons une technique d'analyse volumétrique qui combine le recalage précis d'images médicales 3D, le calcul de déformations non-rigides et l'analyse du champ de déformation. Notre technique d'analyse a deux débouchés : la détection de lésions évolutives et la mesure quantitative des variations de volume. L'originalité de notre approche est de ne nécessiter aucune segmentation *précise* de la lésion, hormis la détermination approximative d'une région d'intérêt, qui peut être automatisée. Nous faisons la distinction entre la transformation des tissus (changement d'intensité de l'image sans déformation) et les effets d'expansion ou de contraction qui reflètent un changement de masse à l'intérieur des tissus, une lésion réelle étant généralement une combinaison de ces deux effets. La méthode est testée avec des séquences d'images 3D synthétiques et est appliquée, dans une première tentative de quantification in-vivo de l'effet de masse, à l'analyse d'un patient réel atteint de sclérose en plaques.

Mots-clé : Analyse du champ de déformation, traitement d'image 3D, grille déformable 3D, Sclérose en plaque, mesure de volume, tumeur, effet de masse, stéréologie

1 Introduction

The precise evaluation of tumor volume variations along time is extremely important (see for example [WSF92, Thi95]):

- for pharmaceutical research, to compare the effects of new drugs on different populations of patients.
- for clinical applications, to determine the exact time when a potentially invasive drug is to be given, or surgery is to be performed.
- for clinical follow-up, to quantify the effects of the drug or surgery along time.

The main source of in-vivo information about tumor growth is 3D Medical Imaging such as Magnetic Resonance (MR) images. Classical techniques (see for example [RCGS94, RHPR96]) consist in delineating the tumor in two 3D images of the patient at two different times t_1 and t_2, which gives two volumes $V_1 = V(t_1)$ and $V_2 = V(t_2)$ to be compared. The volume variation $\Delta V = V_2 - V_1$ is an index of the tumor evolution.

This measurement is difficult to perform for at least two reasons: the first one is delineating in 3D, the second one is delineation errors. Because hundreds or thousands of voxels are to be considered, only (semi-)automatic segmentation tools can be used for routine applications. Among possible automatic segmentation tools are the mathematical morphological operators (erosion, dilation, connected components analysis, ...), or the 3D extension of deformable models (3D snakes, see [CCA92]). In most practical cases however, the a-priori medical knowledge of the physician is indispensable: most of these methods incorporate an interactive initialization and a final interactive adjustment tool. Generally also, the accuracy of the delineation is not subvoxel, hence the uncertainty σ_V on the total volume measurement is very often higher than the volume variation itself ($2\sigma_V > \Delta V$).

The main idea in this paper is to use an analysis method based on a volumetric deformation field to first detect the active lesions and then to evaluate their volume variations. In particular, our volume variation measurement necessitates as input only the designation of a region of interest (ROI) surrounding

the lesion (for example a sphere), or, when it is possible, a segmentation of the lesion which is not requested to be sub-voxel. Because we use a precise 3D rigid registration method, this ROI designation or rough segmentation needs to be performed only in *one* of the two 3D images, or one image of the time sequence to analyze, instead of at each time frame. Rather than a single value ΔV of volume variation, our method provides a kind of "signature", or profile, associated to the tumor growth, from which we propose to quantify different effects that we call the *tissue transformation* and the *tissue deformation*.

First we give a general description of the method and a definition of the tissue transformation and deformation effects. Then we concentrate on the description of the deformation field analysis. We present experimental results with synthesized images to evaluate the performance and test the robustness of our method. Lastly, we apply our method to sequences of 3D images of a patient with a Multiple Sclerosis disease, to evidence and quantify a tissue deformation or *mass effect* at the level of the plaques: an effect which, to our knowledge, has never been quantified in-vivo before.

2 General description

The method is in four steps (see also figure 1):

- the 3D rigid registration of the two successive images.
- the computation of the deformation field between the two registered images.
- the detection of evolving lesions.
- the vector field analysis at the level of each detected lesion to quantify the volume variation.

The most original part of the present work are the last two steps: the vector field analysis for both the detection and the quantification of evolving lesions.

For the first step, which is the computation of a rigid transformation between two 3D images I_1 and I_2, we use the automatic rigid matching method based on extremal points described in [Thi96a]. The accuracy of this method

has been evaluated in [PT95] and is of the order of $1/10^{th}$ of a voxel. We then re-sample one of the two images (let say I_2) into I_2' to make it exactly superimposable to I_1 except of course for the regions of the brain which have changed between the two acquisitions (that is, mainly the lesions).

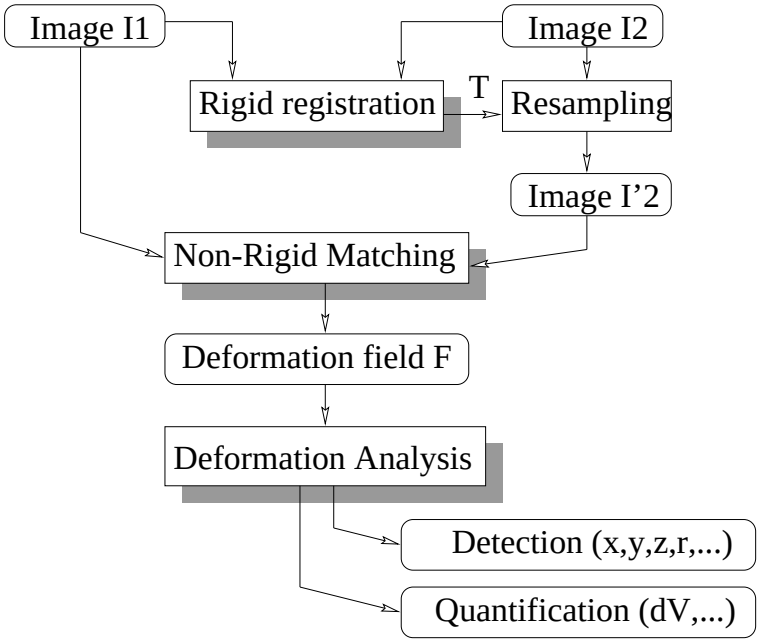

Figure 1: The general principle of the method

We then compute the non-rigid deformation between I_1 and I_2' using the non-rigid matching method described in [Thi96b]. It is a 3D deformable grid technique which is very close to optical flow when small deformations are considered. The result is a deformation field F, represented by a 3D array of displacement vectors, one for each voxel in the image I_1. As in many non-rigid matching methods, the result of the motion field estimation depends on a parameter σ which is a balance between the regularity of the deformation field and the similarity between $I_2'' = F^{-1}(I_2')$ and I_1. It is very unlikely to get rid of this parameter σ which is inherent to any non-rigid matching techniques.

For the "snakes" methods (see [KWT87]), it is the balance between "internal" forces (regularity) and "external" forces (similarity).

This parameter σ has some influence on the volume variation analysis. It can be interpreted to some extent as a blurring of the "real" deformation field, equivalent to a convolution with the Gaussian function $e^{-r^2/2\sigma^2}$ of the vector field (see [Bur81]). This value σ is explicitly defined in the non-rigid matching method that we are using (see [Thi96b]).

The next sections describe in details the detection of evolving lesions and the quantification of volume variation. First, we must define precisely the effects that we want to measure.

3 Tissue deformation and transformation

We distinguish between two different models of tumor growth, real cases being generally a mix of these effects. Our model is crude with respect to many other works existing in the medical domain and concerning the biological aspect of tumor growth (see for example [You59, CWTB95]). In particular, we consider neither explicitly the elastic properties of the brain tissues (see [Dem81]), nor the dynamic aspect of malignant cells growth, but only two fixed time frames, with no (or very few) biological a-priori knowledge. We will see however that even with crude assumptions, solving the problem is not an easy task.

What changes can be observed in a medical image of a lesion? A tumor can be a replacement of cells by another type of cells, an evolution of the molecular structure of the cells, a growing or destruction of cells, or a complex combination of those cases, which might, or might not have the same appearance in Magnetic Resonance (MR) images. Basically, we distinguish between deformation and transformation:

3.1 Tissue deformation

Some tumors can be observed by the way of a large displacement of the tissues (Edema or mass effect) without image intensity changes. Additional molecules or cells penetrate within the tissue, molecules or cells are exchanged with larger or smaller ones, but it might occur that their appearance (the grey level value) in the MRI is the same, mainly because their proton density is the same. Hence

the only visible effect in that case is an expansion, contraction or deformation of the tissues. We call this effect *diffuse* deformation. But it can be also the addition of new untextured material in the central part of the lesion, which reveals through two effects: the growing of a central spot (the "lesion"), and the displacement of the surrounding tissues (the deformation). We call this model *central* deformation.

3.2 Tissue transformation

To the other extent, a tumor can be observed through a change in intensity without any displacement of the tissues. The molecular structure of the tissue is changing, due for example to the replacement of cells by another type of cells which have not the same molecular content but have the same size: the tissue itself is not displaced. This type of tumor is of course much easier to delineate than in the previous case. The "tumor" volume is the area of the MR image where the tissue has a different composition and therefore a different color. It is a known phenomenon for the plaques in T_2 weighted MR images of Multiple Sclerosis: the molecular change corresponds to a demyelination of the axons, and the replacement with molecules with a higher proton density which induces an hyper signal (i.e. a white dot) in the image. Most of the classical tumor measurement methods are based on this model and are using segmentation tools exclusively.

3.3 Defining volume variation measurements

Of course real tumors are always a complex combination of these effects, which makes very difficult to give a clear definition the tumor volume or tumor growth. If central deformation and tissue transformation might present the same appearance in the MRI *within* the lesion itself (i.e. translates into a contrasted central region), they have different influence on the nearest surrounding tissues. This leads to the idea of studying a tumor evolution profile $\Delta V(r)$: a curve representing the volume variation coefficient ΔV as a function of the distance r to the approximate center of the lesion P and up to a limiting bounding radius R. The sphere (P, R) defines a region of interest (ROI) centered on the lesion. By studying the profile $\Delta V(r)$ outside the lesion (but inside

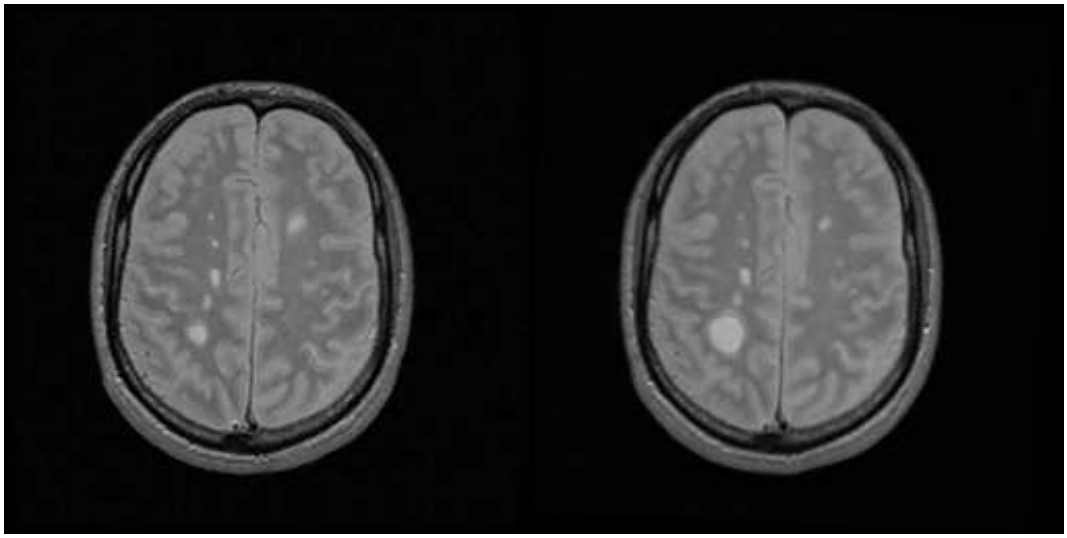

Figure 2: Two registered slices of a real patient with MS disease, and with a two months interval, imaged with first echo T_2 weighted MRI.

the ROI), we might be able to distinguish deformation ($\Delta V(r) = \Delta V$ and $||\mathbf{f}|| \approx 1/r^2$ outside the lesion) from transformation ($\Delta V(r) = 0$ and $||\mathbf{f}|| = 0$ outside the lesion).

3.4 An ideal mathematical solution

Ideally, if we define a virtually closed surface S in the image space, enclosing a region $\mathcal{R}$ of volume V, we can study the flux of tissues through S, represented by the vector field F produced by the non-rigid matching step. Intuitively, the summation of all that goes out minus the summation of all that enters in is equal to the "volume" variation, which is a simplified version of the *Ostrogradsky* theorem, stating that the integral over a closed surface of the flux of a vector field is equal to the integral over the encompassed volume of the divergence of the vector field. In practice, different factors prevent from using directly this mathematically well defined technique. We list now some of these problems with some possible (partial) solutions:

- the vector field F produced by an intensity-based non-rigid matching is equally sensitive to a deformation or a simple intensity change (transformation).

  we can study precisely and separately ideal measurement models for tissue deformation and transformation, test these models on synthetic data, and compare the profiles with those obtained with real data.

- the estimated vector field is inescapably blurred by a regularity parameter σ.

  we can quantify the effect of this blurring on ideal models and measure it in the synthesized models to extrapolate it to real data.

- a lesion can have a shape much more complicated than a sphere.

  we can study a family of imbeded closed surface $\{S_i, i \in [1..m]\}$, encompassing regions $\mathcal{R}_i$ of volume V_i, ranging in size from the approximate center point of the lesion to the complete ROI. It defines a "profile" of the lesion variation $\{\Delta V_i, i \in [1..m]\}$. If the tumor can be approximately segmented, we can use a family of imbeded surfaces whose shapes are much closer to the segmented lesion surface than spherical shells.

- F is not a continuous field, but is sampled for a regular 3D grid (the voxels): it is unclear how to integrate a discrete flow field over a sampled closed surface.

  we develop in this paper a stochastic method to integrate the volume variation from a discrete deformation field.

- the displacement of surrounding tissues induced by a lesion evolution decreases in $(1/r^2)$ outside the lesion, and the vector field evaluation is inherently corrupted by measurement errors and discretization, hence the evaluated flow becomes meaningless very rapidly when we get farther from the lesion. Besides, there might be several active lesions, as in the

case of MS disease.

high frequency noise is eliminated by the regularization of the vector field, but we must keep close to the lesion boundary for meaningful measurements.

- different pathologies exist corresponding to different models of lesions.

  measurements have to be proved useful discrimination tools for each specific type of disease through in-vitro studies and through clinical validations (coherence of the measurements along time, coherence with traditional clinical tests based on external symptoms, coherence with histology, ...).

As we can see, the problem of defining and measuring a precise tumor volume variation is much more complex that simply counting voxels. But even if no complete mathematical formulation is at hand, the precise quantification and its impact on the development of new drugs is too much important to simply give up in front of the difficulty: for the example of multiple sclerosis, there are hundred thousands of patients throughout the world and the cost of a therapy based on β-interferon is very high (nowadays, about \$10000 per year per patient). We describe now the current solutions that we have explored to detect and quantify the evolution of such lesions.

4 Detecting evolving lesions

4.1 Segmentation

As we said previously, detecting lesions in medical images is traditionally performed by segmentation and therefore relies on the local analysis of the intensity or texture in static images. Unfortunately, the intensity is generally not enough specific to automatically characterize a lesion and in most cases several modalities must be used to image the same brain. By combining those different images, for example the first and second echoes of T_2 weighted MR images, it is sometime possible to characterize the lesions in a more robust way, for example by a component classification method (see [GKKK89, CLKJ90]).

Once the lesions are characterized in each time frame, it is then possible to analyse the whole sequence of segmented images as a 4D image (3D + time) and extract and analyse the lesions as 4D connected components (see [MKGV92, KGMW96]). On one hand, this allows to extract static as well as dynamic lesions. On the other hand the motion information is not taken into account in the detection itself.

In the case of Multiple Sclerosis, there are several serious drawbacks in using segmentation methods. In T_2 weighted MR images, the boundary of an MS plaque is fussy, and sometimes surrounded by a halo, hence it is very difficult to segment. The intensity of the plaque is also very close to the intensity of the gray matter, and also of the cerebro-spinal fluid (CSF) of the ventricles. In [KGMW96], this problem is partially overcomed thanks to masking. Besides, thresholding and connected component analysis tools are very unstable operators. For example, an active plaque can merge with a neighboring passive plaque during the expansion: the estimated volume is suddenly and artificially increased due to the capture of the passive plaque or of another brain structure. This prevents from studying precisely and automatically the evolution of individual plaques with segmentation, although it might be possible to obtain some global measurements. Even manually, segmentation is very hard to perform in many cases. At last, the mass effect is totally ignored by segmentation.

4.2 Segmentation of image differences

We propose to use directly the motion in the temporal sequence to characterize active lesions. A simple way is to consider the difference between two consecutive 3D images (see figure 3). When a lesion is characterized by an hypersignal, that is, with an intensity locally larger than the intensity of the surrounding tissues, then a growing lesion appears as a white annulus in the difference of two consecutive images and a shrinking lesion appears as a black annulus. Provided an almost perfect registration of the images, the annulus can be isolated more easily in a difference image than a lesion in a single static image (compare figures 2 and 3).

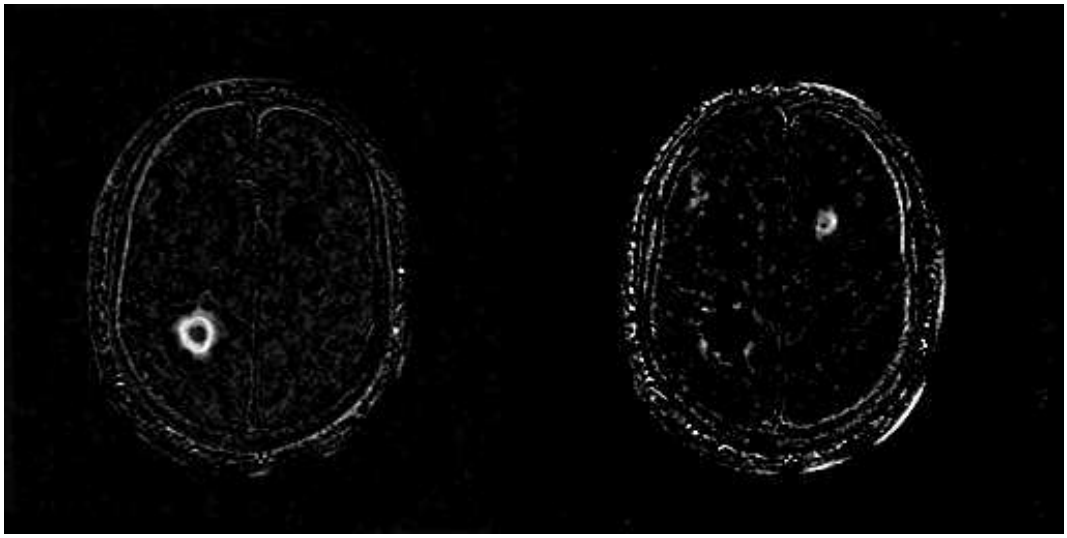

Figure 3: Left, subtraction image: the growing lesion appears as a white annulus. Right, the subtraction image is inverted and a small shrinking lesion can be seen (up right).

4.3 Flow field analysis

We found another, more efficient way to characterize the evolving lesions than image differences: we analyse the deformation field F computed between two consecutive images I_1 and I_2 (see figure 4). F is represented by a discrete function $\mathbf{f}(x, y, z)$, where $\mathbf{f} : (u, v, w)$ is a 3D displacement vector defined at each voxel (x, y, z) of I_1. More precisely, $F(P)$ being the position in I_2 corresponding to a point $P : (x, y, z)$ in I_1, we have:

$$F(P) : \begin{pmatrix} x + u(x, y, z) \\ y + v(x, y, z) \\ z + w(x, y, z) \end{pmatrix} \tag{1}$$

We are interested by places presenting large deformations ($||\mathbf{f}||$ large), and also, as MS plaques have generally a rather spherical shape, places where the divergence $div(\mathbf{f}) = \partial u/\partial x + \partial v/\partial y + \partial w/\partial z$ is large (see figure 5). In

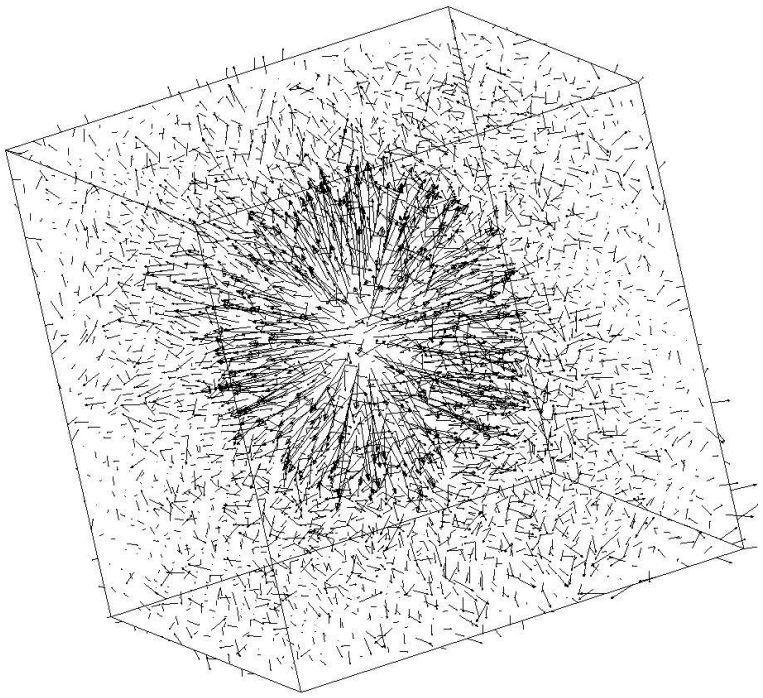

Figure 4: The 3D deformation field measured between the two 3D MRI of the same patient, at the level of the lesion (this lesion is visible in figure 2).

some places $||\mathbf{f}||$ can be large and $|div(\mathbf{f})|$ low (in case of a translation, for example) or $|div(\mathbf{f})|$ can be high and $||\mathbf{f}||$ low (in noisy regions), but as the feature "high magnitude, high divergence" is more specific to evolving lesions, we have tested successfully the following operator $||\mathbf{f}||div(\mathbf{f})$. Besides, the sign of $div(\mathbf{f})$ characterize growing lesions from shrinking lesions. This operator makes active lesions very easy to detect (see figure 5). In addition, in the case of MS plaques, we can use a mask representing the white matter in the brain, because MS plaques appear only in the white matter. We use thresholding and connected component analysis to finally extract automatically the centers and the approximative radii of the active lesions.

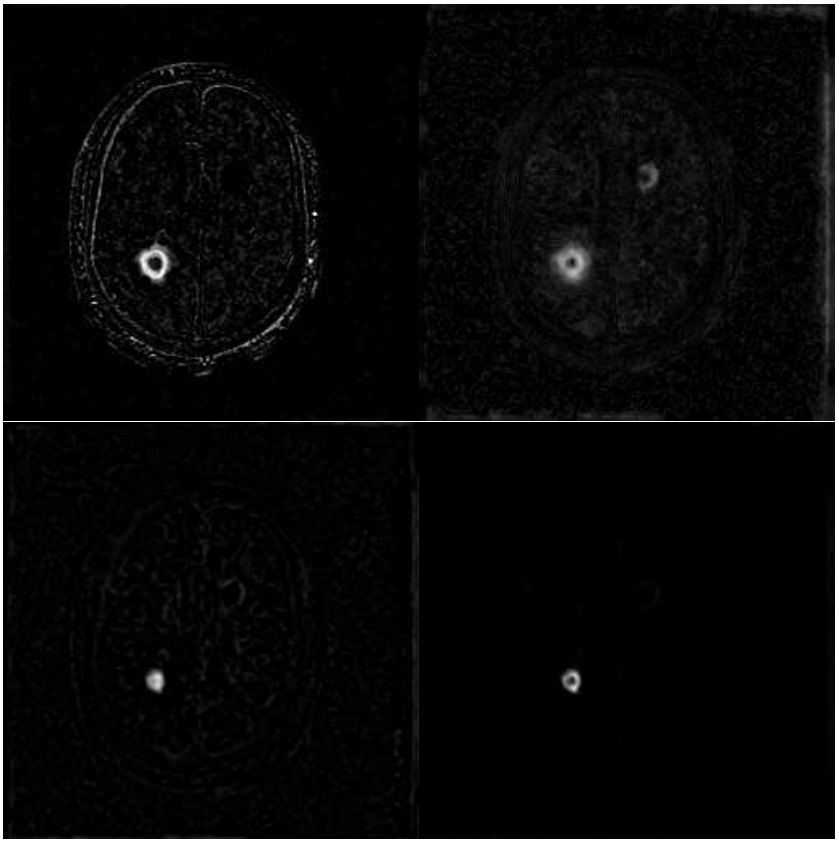

Figure 5: Top left: difference of intensity. Top right: vector field norm $||\mathbf{f}||$. Bottom left: divergence $div(\mathbf{f})$, Bottom right: $||\mathbf{f}||div(\mathbf{f})$. Each step corresponds to an image easier to segment automatically.

5 Measuring the volume variation profile

For now, we assume that the approximate center P and radius R of an active lesion is determined and that we are looking for a precise volume variation measure.

5.1 The method of concentric spheres

In this section, we consider a family of n spheres S_i of increasing radii $\{(P, r_i), r_i \in [0..R]\}$.

5.1.1 Integrating the divergence

A first idea is to compute the integral of the divergence within each sphere S_i, or the integral of the flux on the surface of the sphere which is theoretically equivalent ($\mathbf{n}$ is the normal to the sphere).

$$\Delta V(r_i) = \int_{S_i} \mathbf{f} \cdot \mathbf{n} dS = \int_{V_i} div(\mathbf{f}) dV \tag{2}$$

For a growing lesion, $\Delta V(r_i)$ must increase when i is increased, up to when the lesion is entirely included into (P, r_i): at that point $\Delta V(r_i)$ remains constant. Up to now, however, we didn't get good results in practice with such methods, probably because the noise in the vector field is amplified in the computation of the divergence which necessitates a differentiation.

5.1.2 A stochastic computation

We have then switched to a stochastic method to evaluate the volume variation which is the following.

Assume a shape S, for example a sphere, a cube, or any shape defined by a closed oriented surface in image I_2. Assume also a regular grid G (see figure 6, left). The number of grid nodes times the volume of a single voxel $V(voxel)$ is an approximation of the total volume $V(S)$ of S which tends to the exact value when the grid get thinner. This method is close to stereological methods, which are used to quantify the volumes of static lesions (see [RBBK94]). In the same way, the number of nodes of the regular grid G within the deformed shape $F^{-1}(S)$ gives an approximation of $V(F^{-1}(S))$ (figure 6, right). We note that computing the number of nodes of G within the deformed shape $F^{-1}(S)$ is equivalent to computing the number of nodes of the deformed grid $F(G)$ within the original shape S (figure 6, middle), which is computationally much easier because the deformation F is sampled for each node of G and there is no need to compute the deformed shape $F^{-1}(S)$.

As $F^{-1}(S)$ is the image in I_1 of the shape S in I_2, $\Delta V(S) = V(S) - V(F^{-1}(S))$ is the volume variation between I_1 and I_2 of the shape represented by S in I_2 (or by $F^{-1}(S)$ in I_1).

The method that we propose is fairly simple, but against the intuition: compute the number $N_S(G)$ of nodes of G within S and the number $N_S(F(G))$ of nodes of $F(G)$ also within S. The volume variation $\Delta V(S)$ for the shape S in I_2 is approximately $N_S(G) - N_S(F(G))$. This approximation tends to the exact value when the grid get thinner. If the volume variation is requested for a regular shape within I_1 instead of within I_2, it suffices to use the same method with the inverted transformation F^{-1} obtained for example by the exchange of I_1 and I_2 within the non-rigid matching algorithm.

5.1.3 Practical computation of the profile

Suppose now that we have a family of imbeded shapes $S_i, i \in [0..m]$ such as for example a family of spheres (P, r_i) with increasing radii r_i. We propose an optimal algorithm (i.e with a linear complexity) to compute the volume variation profile. Suppose that we have defined a region of interest (P, R) containing n grid nodes of G:

- we define two arrays of numbers $\{M_i^G\}$ and $\{M_i^{F(G)}\}$, initialized to zero.
- for the n nodes $P_j : (x, y, z)$ of G, we determine the index i of the shell corresponding to the spheres (P, r_i) and (P, r_{i+1}) which contains P_j (resp. $F(P_j)$). i can be obtained in constant time with the distance $d(P_j, P)$ and a lookup table. For each P_j, we increment the corresponding bucket M_i^G (resp. $M_i^{F(G)}$).
- once the arrays $\{M_i^G\}$ and $\{M_i^{F(G)}\}$ are computed, we compute incrementally the arrays $N_i^G = \sum_{k=0}^{i-1} M_k^G$ and $N_i^{F(G)} = \sum_{k=0}^{i-1} M_k^{F(G)}$
- at last, we compute the volume variation profile $\Delta V_i = (N_i^G - N_i^{F(G)}) \times V(voxel)$

The computation complexity of the arrays $\{M_i^G, i \in [0..m-1]\}$ and $\{M_i^{F(G)}, i \in [0..m-1]\}$ is $O(n)$, as for the derivation of $\{N_i^G\}$ and $\{N_i^{F(G)}\}$ from $\{M_i^G\}$

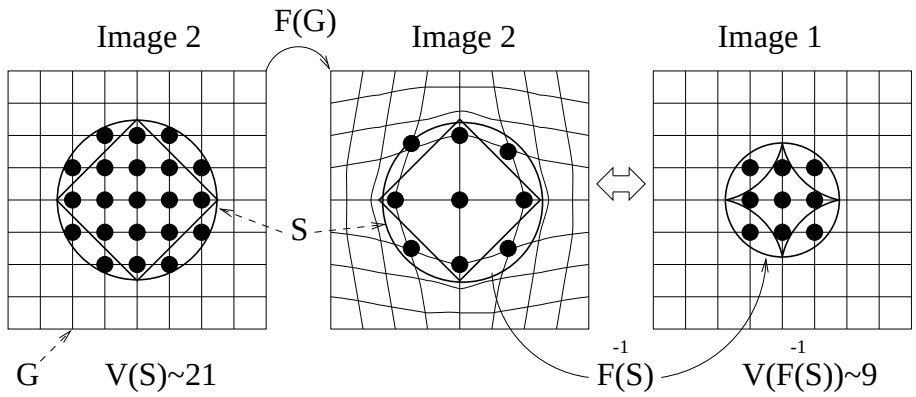

Figure 6: Stochastic computation of the volume variation. The main idea is that the stochastic computation of the volume of a shape $F^{-1}(S)$ with a regular grid G (right) is equivalent to the stochastic computation of S with a deformed grid $F(G)$ (middle).

and $\{M_i^{F(G)}\}$, hence the whole computation of the volume variation profile $\{\Delta V_i, i \in [0..m-1]\}$ is linear ($O(n)$).

We shall note that this computation can also be performed with random positions P_j throughout the region of interest instead of with the nodes of a regular grid G.

5.1.4 Computation of a single value of volume variation

ΔV_i must remain constant and equal to the searched ΔV as soon as r_i is larger than the maximal extent of the lesion. However, because of the noise, ΔV_i moves with a Brownian motion around the true ΔV (each new error increment or decrement the estimated value randomly), which means in practice that ΔV_i oscillates around ΔV with larger and larger amplitudes when i is increased. To avoid this phenomenon, we remove from the computation the effect of very small displacements (when $||\mathbf{f}|| < threshold$ we impose $\mathbf{f} = 0$). With this constraint, the noise is very reduced and ΔV_i tends to zero when r_i becomes large.

In order to get a single value of volume variation, we compute the maximal value $\Delta\bar{V}$ of $\{\Delta V_i, i \in [0..m-1]\}$, which approximates the real ΔV. We have extensively validated this method with synthesized data, which constitutes an important part of the present paper.

5.2 Computing ΔV_i with iso-intensity surfaces

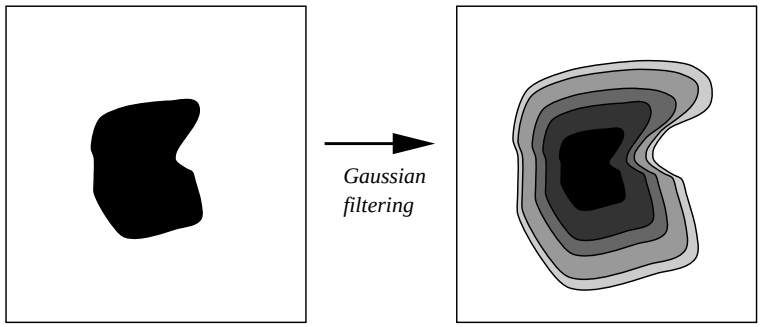

Figure 7: Automatic computation of imbeded surfaces from an approximative segmentation of the lesion.

This method can be improved seriously if we can take into account an approximative shape of the lesion. If the lesion is sufficiently contrasted, it can be segmented as a set of labeled voxels $\mathcal{R}$ in image I_2. In the previous algorithm, we have replaced the spheres (P, r_i) with a family of imbeded closed surfaces $S_i, i \in [0..m]$. A simple way to obtain this family of surfaces is to consider a digital 3D image $I_{\mathcal{R}}$ where the voxels are labeled 0 if they are outside $\mathcal{R}$, or 1 if they are inside. We then blur this image with a Gaussian filter. The iso-intensity surfaces for a set of increasing intensity constants $\{C_i, i \in [0..m], C_i \in [0,1]\}$ have the requested properties (closed and imbeded), and furthermore, the intensity $I(P_j)$ of $I_{\mathcal{R}}$ at a point P_j gives directly the index i of the shell $[S_i, S_{i+1}]$ which contains P_j. Another equivalent solution is to pre-compute a 3D distance map from $\mathcal{R}$, using for example the chamfer distance (see [BTBW77]). The rest of the algorithm is exactly similar to the case of the imbeded spheres, and therefore the whole algorithm has still a linear ($O(n)$) complexity (a few seconds of computation on a workstation).

The segmentation of $\mathcal{R}$ should be distinguished from the precise segmentation used to evaluate the volume variation in traditional methods: it can be much less precise (because it is then blurred), and besides, it must be performed only in one of the two images. If the tumor is well contrasted, using shells around a segmented lesion rather than simple spheres gives more reliable results, because of the fast decrease ($1/r^2$) of the deformation magnitude. Of course, a better segmentation leads to a better deformation analysis. We have verified this assumption with synthetic data.

6 Synthetic experiments

6.1 Tissue Transformation

We suppose (see figure 8) that the tumor evolution is simply a change of intensity without tissue displacement. Another assumption is that the image intensity saturates at the level of the lesion, that is, textural information are lost in those regions.

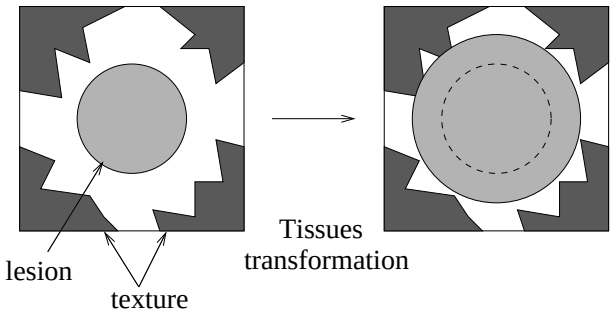

Figure 8: Tissue Transformation: intensity change without tissue displacement.

To produce a synthetic lesion, we have measured the average intensity of plaques in a real MRI, selected a region where the white matter of the brain is homogeneous, and implanted spherical synthetic lesions of known radii in it (see figure 9). The boundaries of the synthetic lesions are blurred to give

a realistic appearance to the false MS plaque. In this model, the deformation field measured by our method is strictly due to intensity changes and not to tissue motion. We have compared the volume variation obtained by our deformation field analysis method based on imbeded spheres, imbeded iso-surfaces and also with segmentation (see table 1).

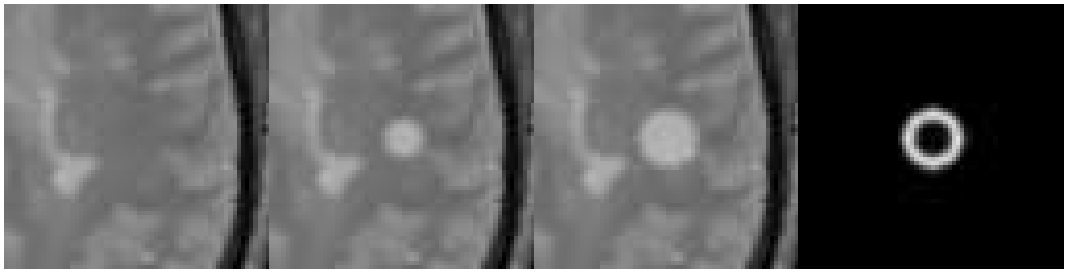

Figure 9: Left to right: original image, synthesized lesion with radius R_1 (I_1), synthesized lesion with radius R_2 (I_2), subtraction $I_2 - I_1$.

The profile ΔV_i for the sphere and for the iso-surface method is presented in figure 10. Note that ΔV_i, which should be zero outside $[R_1, R_2]$ is in fact non-zero because of the regularization of the vector field. The measure which is finally retained is the maximum of ΔV_i, which in that case is a slight overestimation of the real value ΔV. Segmentation seems to perform slightly better than deformation field analysis in that case (see table 1).

6.2 Mathematical model of the expansion field

We now suppose that the lesion is growing in a limited spherical region of radius R_{lesion}, which means that inside this region, the Jacobian determinant J is larger than one. We suppose also that the surrounding tissues are incompressible, which is reasonable for the brain, hence the Jacobian is 1 outside the lesion ($J = 1$). With this model, the expression of the synthetic field is:

$$\mathbf{f}(x,y,z) = \left| \begin{array}{ll} \sqrt[3]{J}.r.\mathbf{n} & \text{if } r < R_{lesion} \\ \sqrt[3]{(J-1)R_{lesion}^3 + r^3}.\mathbf{n} & \text{if } r > R_{lesion} \end{array} \right. \quad (3)$$

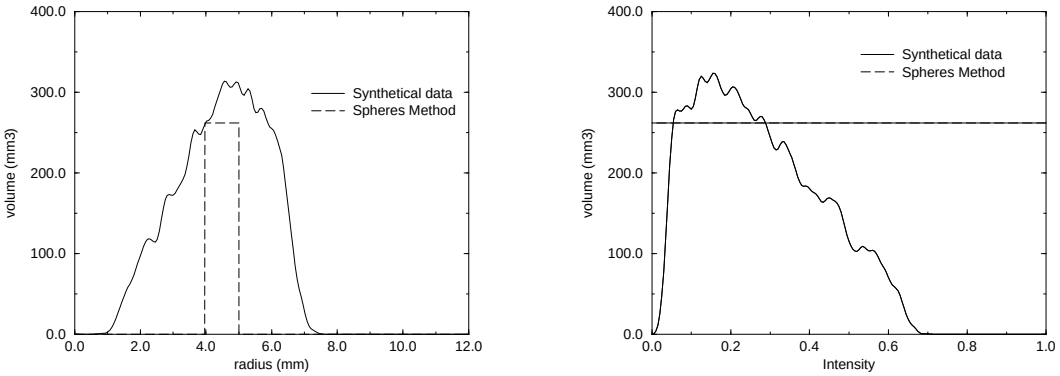

Figure 10: Profile of ΔV_i for tissue transformation: with imbeded spheres (left) and with iso-surfaces (right).

R_1	R_2	ΔV_{th}	ΔV_{sphere}	ΔV_{iso}	ΔV_{seg}
0	3.97	262	245	241	213
0	5	524	375	374	484
0	7.21	1571	880	892	1691
3.97	5	262	314	324	271
5	7.21	1047	1307	1321	1207
3.97	7.21	1309	1435	1404	1478

Table 1: Experiments for tissue transformation: real volume variations (ΔV_{th}), spheres method(ΔV_{sphere}), iso-surfaces method (ΔV_{iso}) and segmentation (ΔV_{seg}).

The theoretical volume variation is then:

$$(J-1)\frac{4}{3}\pi R_{lesion}^3 \tag{4}$$

The invert field (contraction) can be computed from this expression by replacing J with $1/J$ and R_{lesion} with $\sqrt[3]{J}R_{lesion}$. This computation is valid only in dimension 3. The norm of the vector field $||\mathbf{f}||$ is mathematically

equivalent to $1/r^2$ outside $\sqrt[3]{J}R_{lesion}$. It should be noticed that in a 2D world, this field would only decrease in $1/r$, which can contradict our intuition when looking at a 2D slice of a 3D image. We must also remember that we choose to keep the Jacobian constant inside the lesion, but in real cases, the Jacobian could have a complicated profile $J(r)$ with respect to r and can be specific to each pathology.

6.3 Central deformation

Here we suppose that the tumor evolution is the addition of untextured extra-material to the disk of the lesion (see figure 11), therefore, on the contrary to tissue transformation, the lesion is pushing the surrounding tissues.

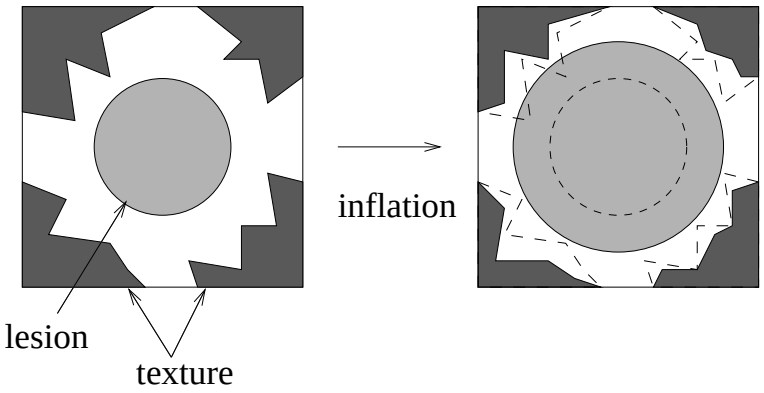

Figure 11: Central deformation: addition of new material in the center of the lesion

To generate synthetic data, we have inlayed a synthetic lesion in the first image (central spot of radius R_{lesion}), computed a synthetic deformation field with a known Jacobian within R_{lesion} and finally applied this field to the first image with a re-sampling algorithm (see figure 12). In the difference image, we note a small motion at the boundary of the brain due to the expansion. This is the only noticeable visible difference with the case of the tissue transformation (compare figure 9 and 12).

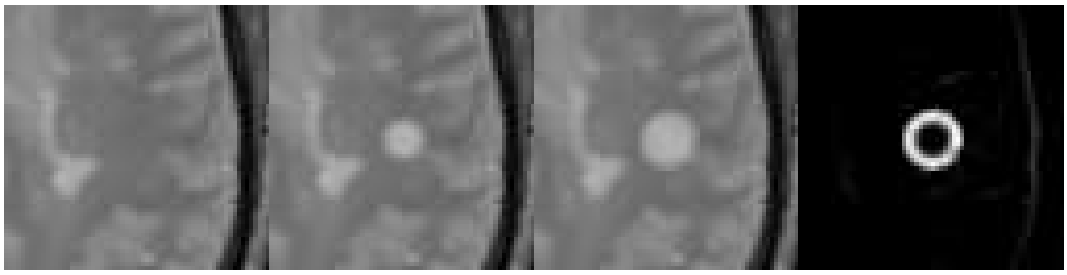

Figure 12: Left to right: original image, synthesized central spot (I_1), synthesized deformation is applied (I_2), subtraction $I_2 - I_1$.

Table 2 presents experimental results comparing real and measured variations with imbeded spheres, imbeded iso-surfaces and segmentation. The segmentation underestimates the volume variation because the synthetic lesion is fussy: the intensity of its boundary is very similar to the one of the underlying image. In that case, the deformation field method gives slightly better results than segmentation. Figure 13 presents an example of measured profile.

Jacobian	ΔV_{th}	ΔV_{sphere}	ΔV_{iso}	ΔV_{seg}
0.5	-262	-265	-270	-258
1.5	262	231	249	200
2	524	454	466	410
3	1047	958	969	872

Table 2: Synthetic experiments for central deformation.

6.4 Diffuse deformation

In this last case, we apply a synthetic deformation field in a region of the image which doesn't present a particular intensity (see figure 14). No segmentation method can be applied at all: the lesion is invisible, even in the subtraction image. Only a slight displacement at the boundary of the brain can be observed (see figure 15). This small shift is the only evidence of an deformation of the

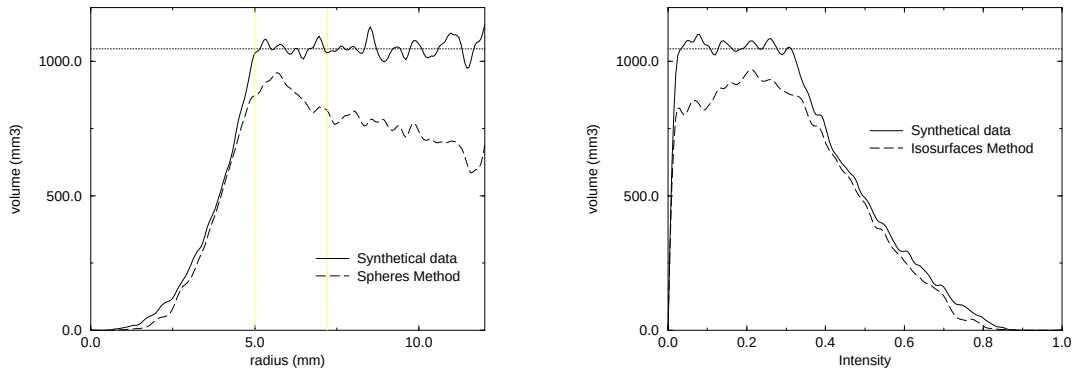

Figure 13: Profile of ΔV_i for central deformation: imbeded spheres method (left) and iso-surfaces method (right). The upper curves are obtained with the synthetic deformation field and the lower curves with the retrieved deformation field and show a slight underestimation.

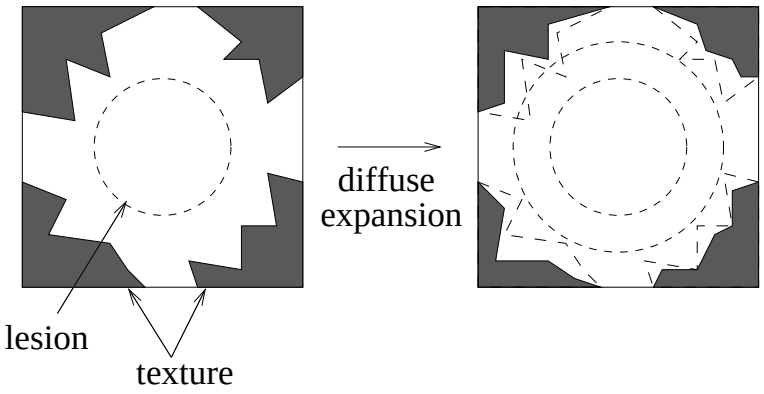

Figure 14: Diffuse deformation: deformation of the tissues without intensity changes.

tissue, which, as we can see, can be partially retrieved thanks to the motion field analysis.

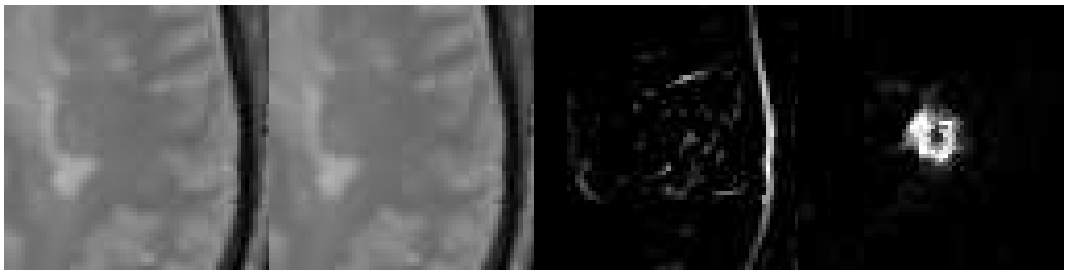

Figure 15: Left to right: original image (I_1), synthesized deformation (I_2), subtraction $I_2 - I_1$ and at last a detection of the lesion is possible thanks to the operator $||\mathbf{f}||div(\mathbf{f})$.

Table 3 shows that the measurements with the deformation field techniques, although underestimating the real volume variation, are interesting indexes to evidence this type of deformation otherwise invisible. Figure 16 shows the associated profile and figure 17 presents the retrieved deformation fields for both central and diffuse deformation.

Jacobian	ΔV_{th}	ΔV_{sphere}	ΔV_{iso}	ΔV_{seg}
0.5	-262	-77	-84	0
1.5	262	142	157	0
2	524	331	365	0
3	1047	720	745	0

Table 3: Synthetic experiments for diffuse deformation.

6.5 Robustness with respect to the approximative center

A very interesting feature of the spheres method is that it is not very sensitive to the precise location of the center P, because, once the sphere is larger than the lesion, the value ΔV_i is theoretically constant (but more and more noisy in practice). We have shifted the center P up to a 3 voxels distance (for a lesion with a diameter of 10 voxels) and measured the performance for the case of

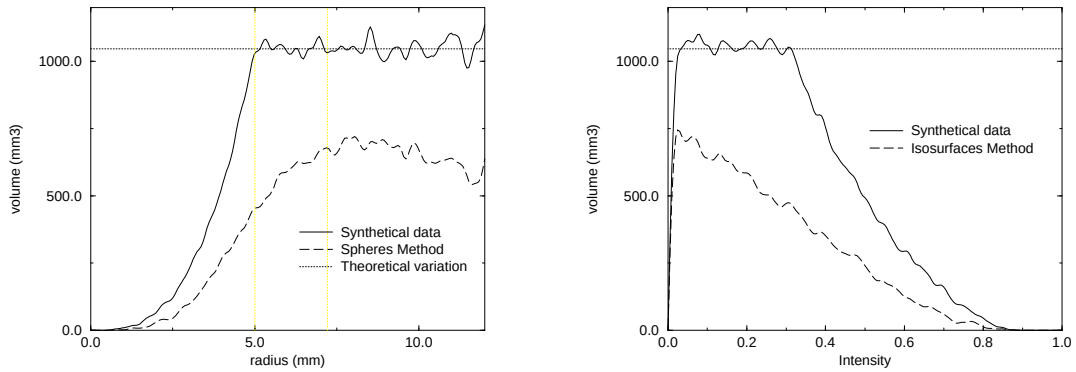

Figure 16: Profile of ΔV_i for diffuse deformation (left: spheres, right: isosurfaces).

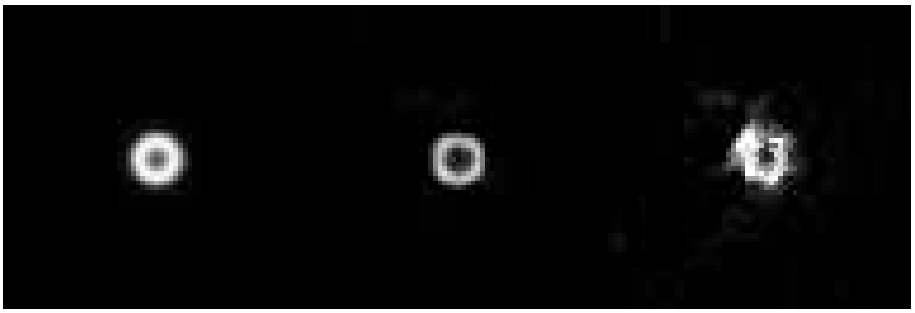

Figure 17: $||\mathbf{f}||div(\mathbf{f})$ computed from the deformation fields. Left to right: synthesized field, retrieved from central deformation images, retrieved from diffuse deformation images. Motion field analysis makes diffuse deformation clearly visible.

central deformation. The results are degraded progressively, but the volume variation measurement is still valuable (see table 4).

Distance d (mm)	$\Delta(v)_{\text{th}}$	$\Delta(v)_{\text{sphere}}$
0.5	524	454
1	524	440
1.5	524	416
2	524	432
2.5	524	410
3	524	414

Table 4: Robustness with respect to the displacement d of the center

6.6 Robustness with respect to shape

It is not an easy task to derive the theoretical deformation field of complex shapes. We have performed experiments with only ellipsoidal lesions and for central deformation, with volume $V = 4/3\pi R_x R_y R_z$. In that case, the results are much better for the iso-surface technique than for the spheres, as one would expect (see table 5).

R_x, R_y (mm)	R_z (mm)	$\Delta(v)_{\text{th}}$	$\Delta(v)_{\text{sphere}}$	$\Delta(v)_{\text{iso}}$
4.368	6.552	524	393	451
3.969	7.937	524	402	484
3.684	9.210	524	343	469

Table 5: Robustness with respect to shape

6.7 Conclusion on synthetic experiments

Segmentation is probably best suited for pure tissue transformation, that is, when the tissues are not displaced, but this model is unlikely to be realistic for actual lesions. When there is a deformation, we can have a continuous variation of cases in between central and diffuse deformation. For central deformation, our method relying on deformation field and a segmentation method can give comparable results. However, the deformation field method becomes much better when the deformation is more important than the intensity changes: in

that case, segmentation underestimates much more the volume variation than the deformation field method, up to the point when segmentation cannot be used anymore (no visible intensity changes).

Hence in real cases, we can expect that if, for a given lesion, the volume variation obtained with the deformation field analysis is much more important than the one measured by segmentation, this is an evidence of a deformation of the tissues, or mass effect, larger than the visible spot which can be segmented.

7 Measurements on real Multiple Sclerosis images.

A close inspection on real MS plaques reveals that, in addition to a clearly visible bright spot in the center, some lesions are surrounded by a cloudy halo, whose intensity can hardly be distinguished from the surrounding white matter. This strongly suggests that MS plaques are in fact larger than their visible central spots.

Another clue for this hypothesis is provided by dynamic sequences of accurately registered 3D images. We have perfectly registered the 3D images of a time sequence of 24 time frames (courtesy of Dr. Ron Kikinis, see figure 18) and we have been able to evidence visually a deformation of the surrounding tissues induced by the lesion. The gyri of the brain are pushed when the lesion is growing, and come back to place when it is then shrinking (growing and shrinking is a normal course for active plaques). What is surprising is that this displacement is visible even very far from the central spot (up to 10 voxels). Because the deformation effect decreases in $1/r^2$ in 3D, the central spot alone cannot explain visible displacement that far from the center. It can be sensitive only 2 or 3 voxels apart and the only explanation that we found is that a diffuse deformation, much larger in extension than the visible spot is responsible of these displacements of tissues.

To give quantitative grounds to this assumption, we have compared the volume variation obtained by segmenting the plaque visible in the 20 images of figure 18, with the results of the spheres and the iso-surfaces method (see table 6 or figure 19). The variations obtained by the deformation field methods are much larger (about twice) than the ones obtained by segmentation, which justifies our hypothesis. We can see also that the spheres and the iso-surfaces

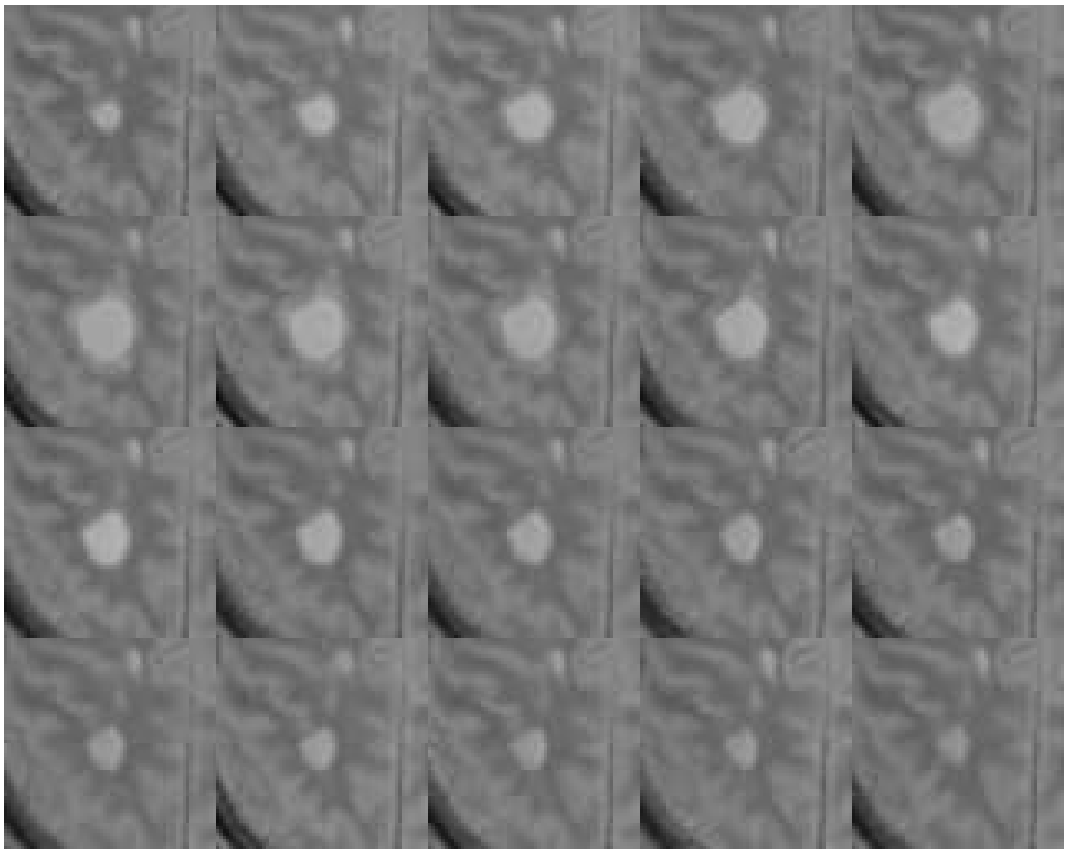

Figure 18: The same region of interest in the 20 successive images of the same patient.

methods give coherent results and that, like in synthetic cases, the iso-surface variations are generally slightly larger. The profiles ΔV_i obtained in the real case nicely follow the theoretical ones (see figure 20) which is an additional confirmation of the validity of our model. As the lesion is not spherical, we believe that the iso-surfaces measurement method is the most reliable. In fact, even a volume variation twice as large as what is measured by segmentation seems to us insufficient to fully explained the visual effect in the dynamic sequence. We saw previously that the iso-surfaces method underestimates

I_i to I_{i+1}	1	2	3	4	5	6	7	8	9	10
ΔV_{seg}	738	876	674	593	356	40	-339	-499	-384	-387
ΔV_{sphere}	1451	1356	915	1114	1594	608	-895	-1792	-812	-1044
ΔV_{iso}	1486	1415	1057	1175	1528	572	-837	-1880	-1027	-1136
t_i to t_{i+1}	11	12	13	14	15	16	17	18	19	
ΔV_{seg}	-342	-312	-432	-174	-308	69	-181	-143	-100	
ΔV_{sphere}	-617	-403	-455	-334	-189	-319	-153	-162.5	-232	
ΔV_{iso}	-738	-351	-583	-386	-182	-87	-141	-183	-161	

Table 6: Measurements of the volume variation with a real plaque (results in mm^3), for the time series of 20 3D images, represented in figure 18.

pure diffuse deformation in synthetic experiments (about a factor 2), hence we believe that the value which is provided by our method is a lower bound of an even larger diffuse deformation.

By integrating the volume variation (see table 7 or figure 21), we can estimate the absolute volume from both the spheres and the iso-surfaces measurements and compare it to segmented volumes. Of course, as for any integration, the error grow each time a new volume difference is taken into account, because the errors are additive. In our experiments, a striking result is that the final error is very reduced. Visually in our time sequence, we start and end with a very small lesion, hence the integral of the volume variation should be close to zero, which is the case in practice, with a final variation of less than $500mm^3$ after the summation of 20 volume variations, to be compared to the $7500mm^3$ of the largest extension. The volume profile obtained from the segmentation and from the deformation field methods are very coherent except for a multiplicative factor, which tends to confirm also that the mass effect is larger than the volume of the spot visible in the MR images.

8 Conclusion

Thanks to an highly accurate 3D registration algorithm and time sequences of 3D images, we had visually observed a diffuse deformation or "mass effect" in

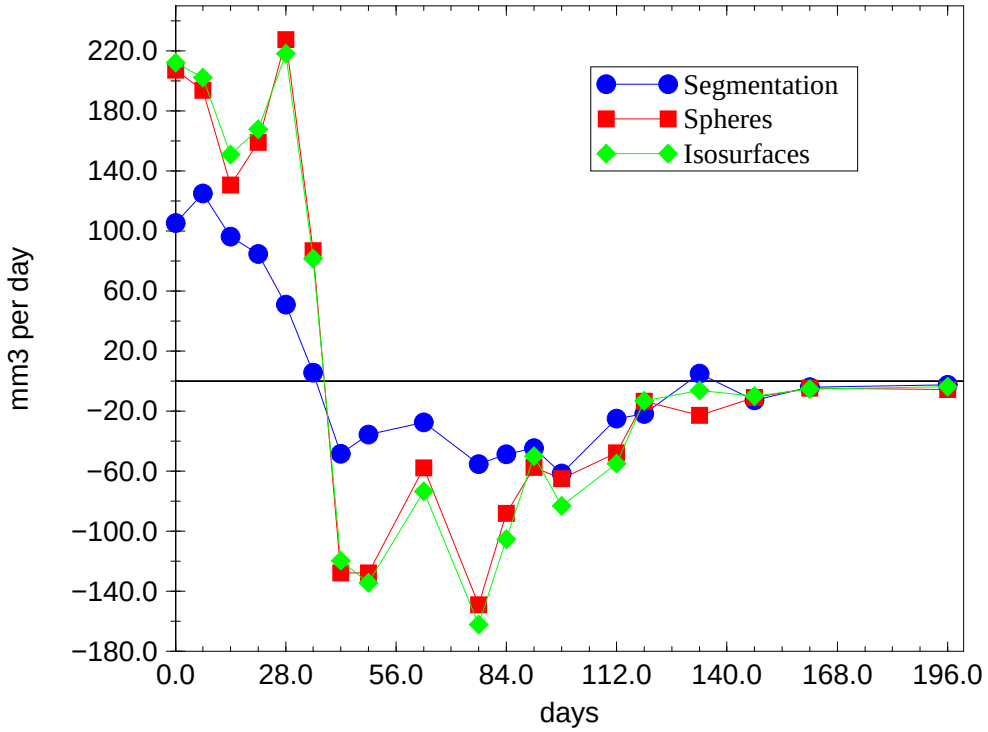

Figure 19: Temporal volume variation (dV/dt) with a real plaque, for the time series of 20 3D images (results in mm^3 per day): comparison of segmentation, spheres method and iso-surfaces method.

the Multiple Sclerosis disease (the eye being a precious tool to perform optical flow analysis). To our knowledge, it is the first attempt to quantify the mass effect in vivo for the MS disease. This first result is extremely promising to better understand the MS disease. Our detection and quantification methods can help also to quantify more precisely the impacts on the MS disease of new drugs (such as β-Interferon) which are now tested in many ongoing clinical

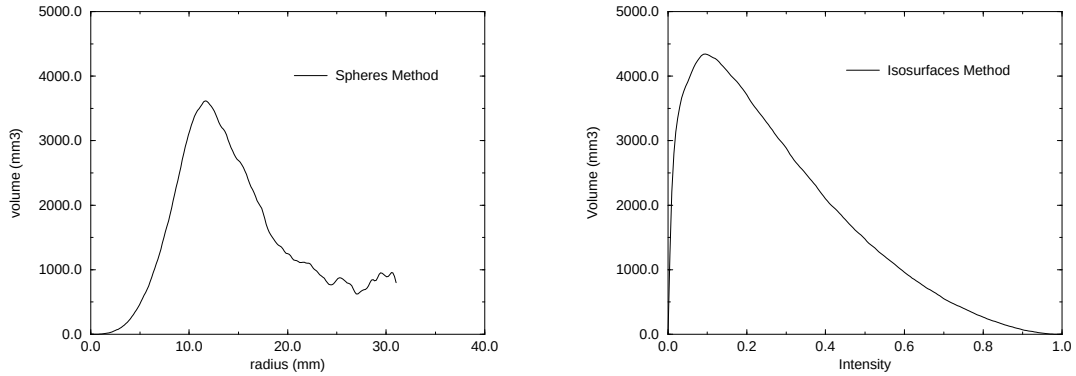

Figure 20: Profile of ΔV_i for real images. Left: measured with the spheres. Right: measured with the iso-surfaces (computed between frame 1 and frame 4).

Image #	1	2	3	4	5	6	7	8	9	10
V_{seg}	350	1088	1964	2638	3231	3587	3627	3288	2789	2405
V_{sphere}	350	1801	3157	4072	5186	6780	7388	6493	4701	3889
V_{iso}	350	1836	3251	4308	5483	7011	7583	6746	4866	3839
Image #	11	12	13	14	15	16	17	18	19	20
V_{seg}	2018	1676	1364	932	758	450	519	338	195	95
V_{sphere}	2845	2228	1825	1370	1036	847	528	375	212	-19
V_{iso}	2703	1965	1614	1031	645	463	376	235	52	-109

Table 7: Estimation of the volume with a real plaque (results in mm^3), for a time series of 20 3D images, represented in figure 18. Note that for the deformation field analysis techniques (spheres and iso-surfaces), this value is obtained by integration from the first value given by the segmentation, hence can be subject to increasing errors.

trials. The application of our tool, however, is not limited to Multiple Sclerosis plaques, but might be applied to the study of many other types of lesions

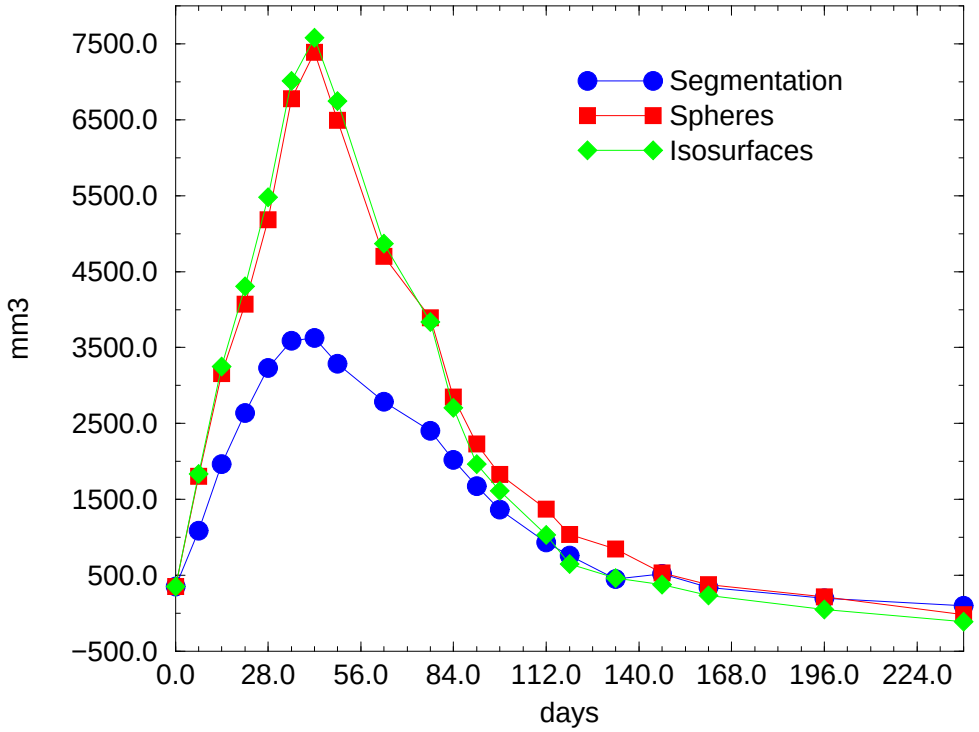

Figure 21: Volume of a real plaque for the time series of 20 3D images: comparison of segmentation, spheres method and iso-surfaces method

such as cancer tumors.

Acknowledgment

Many thanks to Dr. Ron Kikinis and Dr. Charles Guttmann, Brigham and Women's Hospital, Harvard Medical School, Boston and to Dr. Neil Roberts, MARIARC, University of Liverpool, who provided us with temporal sequences

of MS diseased patients. This study is also related to the EC Biomed II project BIOMORPH.

References

[BTBW77] H.G. Barrow, J.M. Tenenbaum, R.C. Bolles, and H.C. Wolf. Parametric correspondence and chamfer matching: Two new techniques for image matching. In *Proc. of the 5th international Joint Conference on Artificial Intelligence*, pages 659–663, Cambridge, MA, 1977.

[Bur81] D.J. Burr. A dynamic model for image registration. *Computer Graphics and Image Processing*, 15(2):102–112, February 1981.

[CCA92] Isaac Cohen, Laurent Cohen, and Nicholas Ayache. Using deformable surfaces to segment 3d images and infer differential structures. *CVGIP : Image understanding '92*, September 1992.

[CLKJ90] H.E. Cline, W.E. Lorensen, R. Kikinis, and F. Jolesz. Three-dimensional segmentation of mr images of the head using probability and connectivity. *JCAT*, 14(6):1037–1045, 1990.

[CWTB95] Gerhard C. Cruywagen, Diana E. Woodward, Philippe Tracqui, Grace T. Bartoo, J.D. Murray, and Ellsworth C. Alvord. The modelling of diffusive tumours. *Journal of Biological Systems*, 3(4):937–945, 1995.

[Dem81] H. Demiray. Large deformation analysis of some soft biological tissue. *Journal of Biomechanical Engineering*, 103:73–78, May 1981.

[GKKK89] G. Gerig, W. Kuoni, R. Kikinis, and O. Kübler. Medical image and computer vision: an integrated approach for diagnosis and planning. pages 425–443, Springer, 1989.

[KGMW96] R. Kikinis, C. Guttmann, D. Medcalf, W. Wells, G. Ettinger, H. Weiner, and F. Jolesz. *Quantitative Follow-up of Patients with Multiple Sclerosis using MRI Part I: Technical Aspects.* Technical Report 40, Surgical Planning Laboratory, Brigham and Women's Hospital, Harvard Medical School, Boston, USA, October 1996.

[KWT87] Michael Kass, Andrew Witkin, and Demetri Terzopoulos. Snakes: Active contour models. *International Journal of Computer Vision*, 1:312–331, 1987.

[MKGV92] D. Medcalf, R. Kikinis, C. Guttmann, L. Vaina, and F. Jolesz. 4d connected component labelling applied to quantitative analysis of ms lesion temporal development. october 1992.

[PT95] X. Pennec and J.P. Thirion. Validation of 3-d registration methods based on points and frames. In *Proceedings of the 5th Int. Conf on Comp. Vision (ICCV95)*, pages 557–562, Cambridge, MA, June 1995.

[RBBK94] Neil Roberts, Silas Barbosa, Lance D. Blumhardt, Ron A. Kowaski, and Richard H.T. Edwards. Stereological estimation of the total volume of mr visible brain lesions in patients with multiple sclerosis. *MAGMA*, 2:375–378, 1994.

[RCGS94] S.A. Roll, A.C.F. Colchester, L.D. Griffin, P.E. Summers, F. Bello, B. Sharrack, and D. Leibfritz. Volume estimation of synthetic multiple sclerosis lesions : An evaluation of methods. In *3rd Annual Meeting of the Society of Magnetic Resonance*, page 120, Nice, France, August 1994. (held jointly with the 12th Annual Meeting of the European Society of Magnetic Resonance in Medicine and Biology).

[RHPR96] C. Roszmanith, H. Handels, S.J. Pöppl, E. Rinast, and H.D. Weiss. Characterization and classification of brain tumours in three-dimensional mr image sequences. In *Visualization in Biomedical Computing, VBC'96*, Hamburg, Germany, September 1996.

[Thi95] J-P Thirion. Software to assist in monitoring treatment. In *IBC's 3rd Annual Multiple Sclerosis Conference*, Boston, May 1995.

[Thi96a] J-P Thirion. New feature points based on geometric invariants for 3d image registration. *International Journal of Computer Vision*, 18(2):121–137, May 1996.

[Thi96b] J-P Thirion. Non-rigid matching using demons. In *Computer Vision and Pattern Recognition, CVPR'96*, San Francisco, California USA, June 1996.

[WSF92] Carla J. Wallace, T. Peter Seland, and T. Chen Fong. Multiple sclerosis : The impact of m.r. imaging. *AJR*, 158:849–857, April 1992.

[You59] J.S. Young. The invasive growth of malignant tumours : an experimental interpretation based on elastic-jelly models. *The Journal of Pathology and Bacteriology*, 77(2):321–339, 1959.

Unité de recherche INRIA Lorraine, Technopôle de Nancy-Brabois, Campus scientifique,
615 rue du Jardin Botanique, BP 101, 54600 VILLERS LÈS NANCY
Unité de recherche INRIA Rennes, Irisa, Campus universitaire de Beaulieu, 35042 RENNES Cedex
Unité de recherche INRIA Rhône-Alpes, 655, avenue de l'Europe, 38330 MONTBONNOT ST MARTIN
Unité de recherche INRIA Rocquencourt, Domaine de Voluceau, Rocquencourt, BP 105, 78153 LE CHESNAY Cedex
Unité de recherche INRIA Sophia Antipolis, 2004 route des Lucioles, BP 93, 06902 SOPHIA ANTIPOLIS Cedex

Éditeur
INRIA, Domaine de Voluceau, Rocquencourt, BP 105, 78153 LE CHESNAY Cedex (France)
ISSN 0249-6399